

退火气氛对氧化镓薄膜结构及特性的影响

陶志文¹, 毛梓宁², 许佳雄^{2*}¹广东工业大学材料与能源学院, 广东 广州 510006;²广东工业大学集成电路学院, 广东 广州 510006

摘要 通过溶液法在石英玻璃衬底上制备氧化镓(Ga_2O_3)薄膜,研究氮气、空气和氧气气氛退火的 Ga_2O_3 薄膜的结构、光学特性、缺陷能级与电学特性。结果表明,氮气气氛退火的 Ga_2O_3 薄膜的形貌组织最致密均匀且最厚,氧气气氛退火的薄膜结晶度最优。所有样品在可见光区的平均透光率均高于80%,且在260 nm附近都出现陡峭的吸收边,在190 nm处透光率均低于10%,氮气、空气和氧气气氛退火的 Ga_2O_3 薄膜的禁带宽度分别为5.10 eV、5.07 eV和5.18 eV。氮气、空气、氧气气氛退火的样品在蓝-紫外波段的光致发光强度依次降低。根据光致发光谱分析 Ga_2O_3 薄膜缺陷能级, Ga_2O_3 的施主能级到导带的距离随着禁带宽度值的增大而增大。氮气、空气、氧气气氛退火的样品电阻依次增大。本文实验中最优退火气氛为氮气。

关键词 薄膜; 氧化镓薄膜; 退火气氛; 溶液法; 缺陷能级; 薄膜特性

中图分类号 O484 **文献标志码** A

DOI: 10.3788/AOS231326

1 引言

第四代半导体材料氧化镓(Ga_2O_3)具有较大的带隙(4.5~5.3 eV)、击穿电场强度(8 eV/cm)、Baliga品质因数(70.7 MW/cm²),较好的热稳定性,以及合适的光吸收特性等优点,在功率器件、日盲紫外探测等方面的应用有着得天独厚的优势^[1]。

大部分文献报道以脉冲激光沉积、化学气相沉积和射频溅射等方法制备 Ga_2O_3 薄膜^[2-5],采用溶液法制备 Ga_2O_3 薄膜的报道相对较少^[6-7]。脉冲激光沉积和射频溅射法需要昂贵的设备,化学气相沉积法的沉积速率较低,而溶液法具有低环境负荷和成本、操作简单等优点。Park等^[6]通过溶液法在石英衬底上制备 Ga_2O_3 薄膜,研究干燥温度和起始溶液的摩尔浓度对 Ga_2O_3 薄膜的影响,Yu等^[7]采用溶胶-凝胶法合成 Ga_2O_3 薄膜,但薄膜结晶度较低,且对日盲紫外光的吸收性较差。

前驱体溶液的杂质含量、 Ga^{3+} 浓度、薄膜干燥温度、退火温度及气氛影响 Ga_2O_3 薄膜的杂质含量、结晶度及表面形貌,从而影响材料的光学及电学特性。为了尽量减少溶液存在的杂质,本文通过采用带有两个氨基的1,2-丙二胺作为稳定剂减少了稳定剂添加量,通过制备高 Ga^{3+} 浓度的前驱体溶液减少了溶剂添加量。采用较高的干燥温度及退火温度来提高薄膜结晶

度。本文研究氮气、空气和氧气三种气氛退火的 Ga_2O_3 薄膜的结晶特性、表面形貌、光学特性、带隙及电学特性,并分析 Ga_2O_3 的缺陷能级。

2 实验

2.1 材料的制备

将0.02 mol(质量为5.1148 g)的硝酸镓水合物(纯度为99.9%)溶于9 mL乙二醇单甲醚(分析纯)中,通过室温搅拌形成透明溶液, Ga^{3+} 的摩尔浓度为2.0 mol/L;接着加入0.01 mol(体积为0.9 mL)的1,2-丙二胺(纯度为99%),经约2 h的50 °C水浴加热搅拌,过滤得到黄色透明前驱体溶液。

采用旋涂法在石英片($\Phi 15\text{ mm} \times 1\text{ mm}$)上制备薄膜。制膜前,将衬底依次放在去离子水、丙酮、无水乙醇、去离子水中各超声清洗10 min。旋涂时匀胶机(EZ4)匀胶速率设定为5000 r/min,运行时间为20 s。匀胶结束后,将样品置于烘胶机(SC-H)上进行200 °C干燥处理。待有机溶剂挥发后,重复旋涂、干燥4次。

采用管式退火炉(NBD-O1200)分别在氮气、空气、氧气气氛中对样品进行退火处理。根据前期实验结果,本文采用的退火温度为1100 °C,退火时间为1 h,升温速率为10 °C/min。退火结束后样品随炉冷却。

收稿日期: 2023-07-27; 修回日期: 2023-08-30; 录用日期: 2023-09-06; 网络首发日期: 2023-09-22

基金项目: 广东省科技计划项目(2017A010104017)

通信作者: *xujiaxiong@gdut.edu.cn

2.2 样品表征与性能检测

通过 D/MAX-Ultima IV 型 X 射线衍射 (XRD) 仪 (Cu K_{α} , 波长 $\lambda=0.154$ nm) 分析薄膜晶体结构。采用 SU8010 型冷场发射扫描电子显微镜 (SEM) 表征薄膜形貌。采用 UV-3600 Plus 型紫外-可见-近红外分光光度计采集薄膜的透射光谱和反射光谱。使用 Fluorolog-3 型荧光分光光度计测量薄膜的光致发光 (PL) 谱, 选定激发光波长为 240 nm。进行电流-电压 (I - V) 特性测试前采用小型离子溅射仪 (SBC-12) 结合掩模版在 Ga_2O_3 薄膜表面溅射约 100 nm 厚的 6 对平面 Au 叉指电极, 每个电极的指长为 5000 μm , 指间距为 300 μm , 指宽为 200 μm ; 采用 Keithley 2635B 型源表结合探针台扎针接触 Au 叉指电极, 测试 Ga_2O_3 薄膜的 I - V 特性曲线。

3 分析与讨论

图 1(a) 为不同气氛下退火的样品 XRD 谱图。三种气氛退火的样品 XRD 谱都与 Ga_2O_3 标准卡片匹配, 其中 (400) 和 (-202) 晶面处的衍射峰较强, 其他衍射

峰较微弱, 这可能是由于 (400) 和 (-202) 晶面的表面能低于其他晶面, 因此薄膜更易趋向 (400) 和 (-202) 晶面生长, 以降低系统的总能量。在 21.5° 处的馒头峰来源于石英片。对比不同样品的 XRD 谱可见: 除 Ga_2O_3 (400) 晶面的衍射峰外, 氮气、空气、氧气气氛退火样品 XRD 谱中各衍射峰强度依次减弱; 氮气和氧气气氛退火薄膜的 (400) 晶面相对于 (-202) 晶面的取向优势较明显, 而空气气氛退火薄膜的 (400) 晶面相对于 (-202) 晶面的取向优势不明显, 这说明在空气气氛退火过程中, 空气中的杂质会影响薄膜 (400) 晶面的生长。采用谢乐公式 [$G=k\lambda/(F\cos\theta)$, 其中, G 为平均结晶尺寸, k 为形状系数, λ 为 X 射线波长, F 和 θ 为 (400) 晶面衍射峰的半峰全宽和布拉格角度] 计算 Ga_2O_3 的结晶尺寸^[8]。图 1(b) 为 Ga_2O_3 的结晶尺寸随退火气氛的变化图。在氮气、空气和氧气气氛退火后, Ga_2O_3 薄膜平均结晶尺寸分别为 23.5 nm、24.9 nm 和 28.1 nm, 在氧气气氛退火的样品结晶度最高, 在氮气气氛退火的样品结晶度最低, 这可能是由于: 充足的氧气气氛退火利于对 Ga_2O_3 晶格中氧空位的补偿, 从而促进结晶。

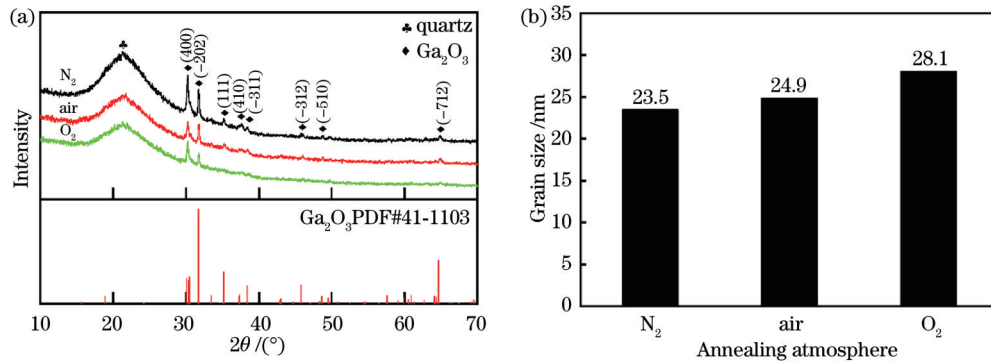


图 1 不同气氛下退火的 Ga_2O_3 薄膜 XRD 结果。(a) XRD 谱图; (b) 结晶尺寸

Fig. 1 XRD results of Ga_2O_3 films annealed in different atmospheres. (a) XRD pattern; (b) crystal size

图 2 为不同气氛退火样品的表面与截面 SEM 图。观察表面 SEM 图可见, 3 种气氛退火的 Ga_2O_3 薄膜均由不规则的颗粒组成。空气、氮气、氧气气氛退火薄膜的颗粒大小依次递增, 空气气氛退火的薄膜孔隙最多, 氮气气氛退火的薄膜致密性最好, 形貌组织更均匀。由截面 SEM 图可知, 氮气气氛退火的 Ga_2O_3 薄膜厚度最大且最均匀, 氮气、空气、氧气气氛退火的薄膜厚度依次减小, 分别为 222 nm、178 nm、112 nm, 这解释了在 XRD 结果中衍射峰强度依次减弱的现象。三者薄膜厚度依次减小的原因是: 1100 °C 的高温退火可能会使薄膜发生升华, 氧气气氛促进升华的发生。由此可见, 氮气气氛退火能够得到致密均匀且较厚的 Ga_2O_3 薄膜。

图 3 为不同样品的 UV-Vis 测试结果, 其中图 3(a) 为空白石英片的透射光谱, 图 3(b) 为用空白石英片扫基线、扣除石英片影响之后 Ga_2O_3 薄膜本身的透射光谱图。从图 3(b) 中透射光谱可以看出, 3 个样品在可

见光波段的透射率均在 80% 以上, 而对 190 nm 的紫外光的透射率低于 10%, 透射光谱在 260 nm 附近都出现了陡峭的吸收边, 说明样品对日盲紫外光具有较好的选择吸收性, 可应用于日盲紫外光电探测器或滤波片。氮气气氛退火的样品在 300~800 nm 波段的透射率最低, 这可能是薄膜内部较多的缺陷对该波段光的吸收与散射所导致的结果。由 Ga_2O_3 薄膜反射光谱 [图 3(c)] 可以看出, 氧气、氮气和空气气氛退火的 Ga_2O_3 薄膜对紫外-可见光的反射率不超过 3.5%, 其反射率平均值依次减小, 分别为 1.9%、1.5%、1.4%, 这可能与形貌组织等有关。当入射光照射到平滑透明的半导体薄膜上, 应考虑入射光的多次反射, 薄膜的透射率 T 表示为 $T=(1-R)^2e^{-\alpha d}$, 其中 R 为反射率, d 为样品厚度。对于直接带隙材料, T_{auc} 公式为 $(\alpha hv)^2=A(hv-E_g)$, 其中 $h\nu$ 为光子能量, A 为比例常数, E_g 为禁带宽度。作出 $(\alpha hv)^2$ 和 $h\nu$ 的关系曲线图 [图 3(d)], 由线性部分延长线与 x 轴的截点可估算 E_g 值。氮气、

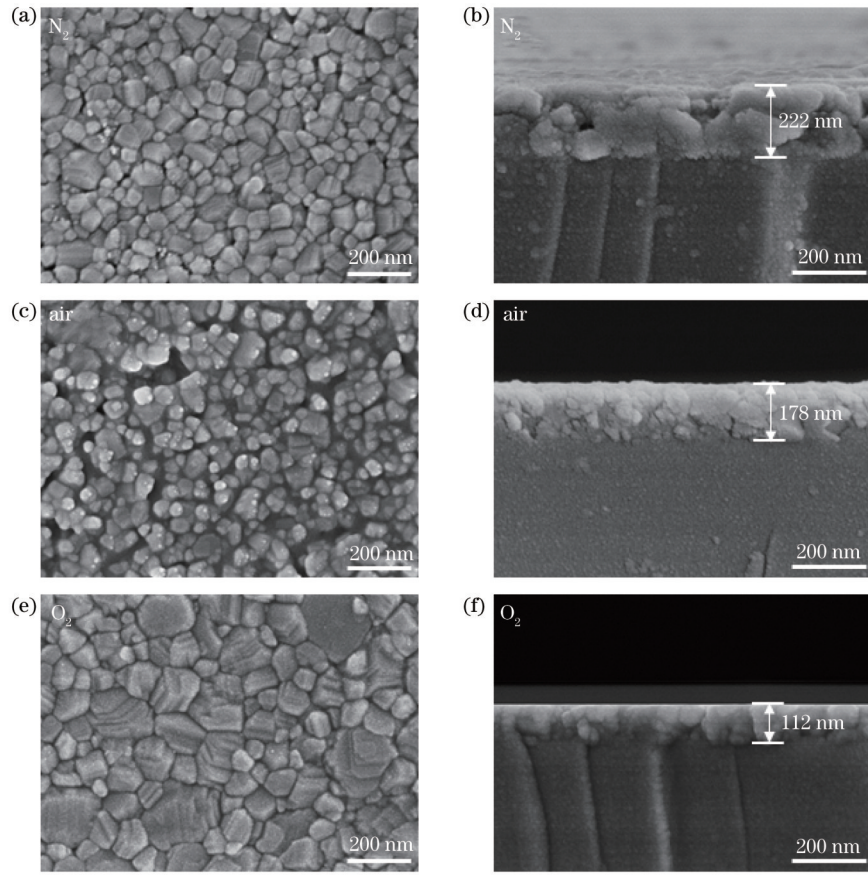


图 2 在不同气氛退火后的样品 SEM 图。(a)(c)(e)Ga₂O₃薄膜表面形貌图;(b)(d)(f)样品的截面形貌图

Fig. 2 Annealed SEM images for different gas. (a)(c)(e) Surface topographies of Ga₂O₃ films; (b)(d)(f) cross-section images of Ga₂O₃ films

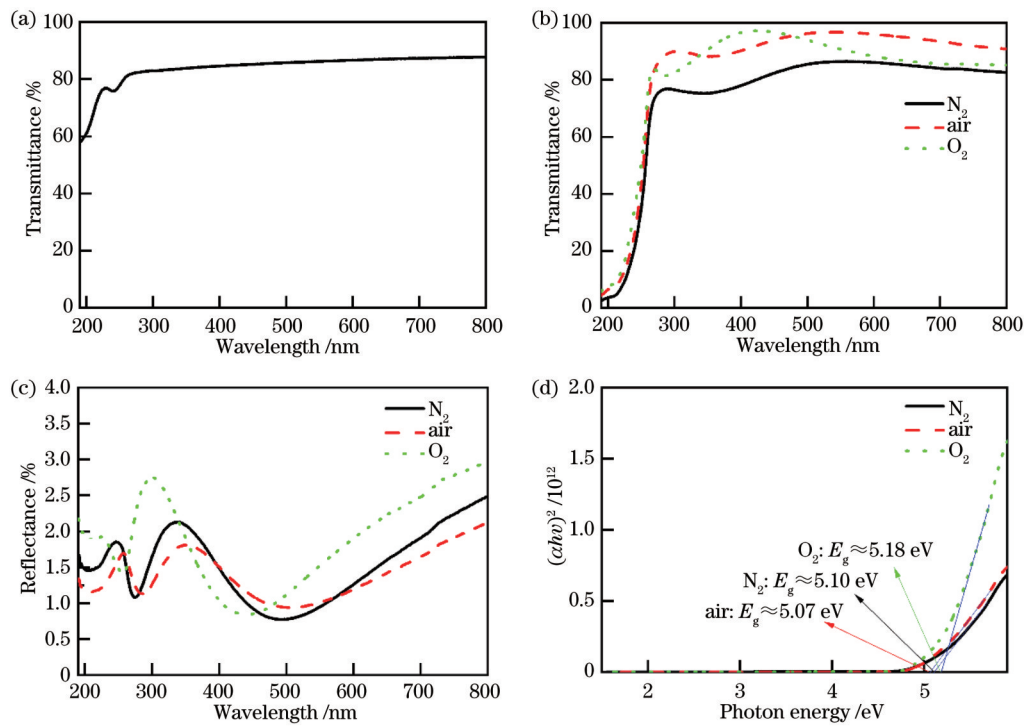


图 3 不同样品的 UV-Vis 测试结果。(a)石英片的透射光谱;(b)Ga₂O₃薄膜透射光谱;(c)Ga₂O₃薄膜反射光谱;(d) $(\alpha h\nu)^2$ 和 $h\nu$ 的关系曲线

Fig. 3 UV-Vis results of different samples. (a) Transmission spectrum of quartz sheet; (b) transmission spectra of Ga₂O₃ films; (c) reflection spectra of Ga₂O₃ films; (d) relationship between $(\alpha h\nu)^2$ and $h\nu$

空气和氧气气氛退火的样品 E_g 值分别为 5.10 eV、5.07 eV 和 5.18 eV。 E_g 与薄膜的氧空位浓度有关,高浓度的氧空位不可避免地会使价带顶部的陷阱态延伸到禁带,导致带隙缩小^[7]。使用氧气气氛退火时,氧气对 Ga_2O_3 薄膜中氧空位有一定程度的补偿,使 Ga_2O_3 薄膜中氧空位浓度减小,从而增大 E_g 值。

为了分析不同气氛退火的 Ga_2O_3 薄膜内部缺陷的变化情况,对各样品进行 PL 测试,图 4 为 Ga_2O_3 薄膜在 370~600 nm 波段的光致发光谱。 Ga_2O_3 的光致发光一般来源于施主能级上电子和受主能级上空穴的辐射复合,施主能级由氧空位形成,而受主能级可以由镓空位形成,也可以由镓-氧空位对形成^[9]。从图 4 中可以看出,3 个样品在 396 nm、450 nm、468 nm、483 nm、492 nm 和 558 nm 处均有发光峰。其中,氮气气氛退火的 Ga_2O_3 薄膜发光强度最强,说明该样品内部参与辐射复合的缺陷最多^[9-11],这可能来源于薄膜的低结晶度导致的薄膜增多的镓空位或氧空位缺陷;氧气气氛退火的薄膜发光强度最低,说明氧气气氛退火能够减少 Ga_2O_3 薄膜参与辐射复合的缺陷,有效抑制紫外-蓝光波段的发光。

以氮气气氛退火样品为例分析 Ga_2O_3 薄膜的缺陷能级,如图 5 所示。图中 D_1 、 D_2 、 D_3 和 D_4 是 4 个施主态缺陷能级, A_1 和 A_2 是 2 个受主态缺陷能级。根据 Binet 等^[9] 的研究结果,第一淬灭区域的激活能 $\Delta E_1 \approx 0.05$ eV, $E_{D_1} = 0.04$ eV (E_{D_x} 为施主能级 D_x 的能量, $x=1, 2, 3, 4$, 下同) 接近第一淬灭区域的激活能;第二淬灭区域的激活能 $\Delta E_2 \approx 0.42$ eV, 根据乌尔巴赫-费勒定律得出 $E_{A_1} = 0.30$ eV (E_{A_y} 为受主能级 A_y 的能量, $y=1,$

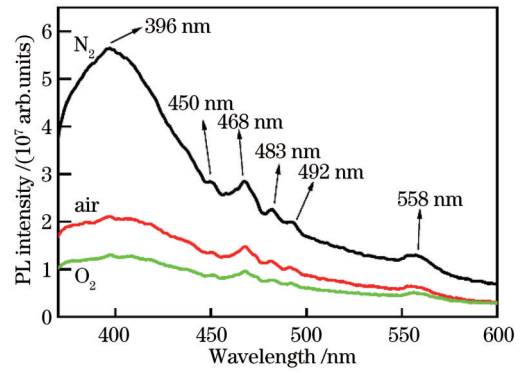


图 4 不同退火条件下制备的 Ga_2O_3 薄膜的室温光致发光谱
Fig. 4 Room temperature photoluminescence spectra of Ga_2O_3 films prepared under different annealing conditions

2, 下同), A_1 由镓-氧空位对形成。进一步根据 Su 等^[12] 的分析方法可以得出各缺陷能级的能量。由 $E_{D_4} = E_g - E_{A_1} - E_{396\text{ nm}}$ ($E_{xxx\text{ nm}}$ 为 xxx nm 光子的能量, 下同) 得到 $E_{D_4} = 1.67$ eV; 通过 $E_{A_2} = E_g - E_{D_4} - E_{558\text{ nm}}$ 计算出 $E_{A_2} = 1.21$ eV, A_2 由镓空位形成。此外, $E_{D_2} = E_g - E_{A_2} - E_{450\text{ nm}} = 1.14$ eV, $E_{D_3} = E_g - E_{A_2} - E_{468\text{ nm}} = 1.25$ eV。根据 Dong 等^[10] 的研究, Ga_2O_3 晶胞中存在三种氧空位, 图 5 中的 D_2 、 D_3 和 D_4 分别由三种氧空位形成。同理可得其他样品的能级分布情况如表 1 所示。氧气气氛退火的样品较大的 E_g 导致施主能级 D_2 、 D_3 和 D_4 的电离能的增大, 施主能级上的电子难以被激发跃迁至导带。所有样品的受主能级 A_1 和 A_2 的电离能都较大, 属于深受主能级, 因此难以实现 P 型导电^[13]。虽然施主能级 D_1 靠近导带, 但施主能级 D_2 、 D_3 和 D_4 远离导带, 因此 Ga_2O_3 薄膜呈现弱 N 型导电。

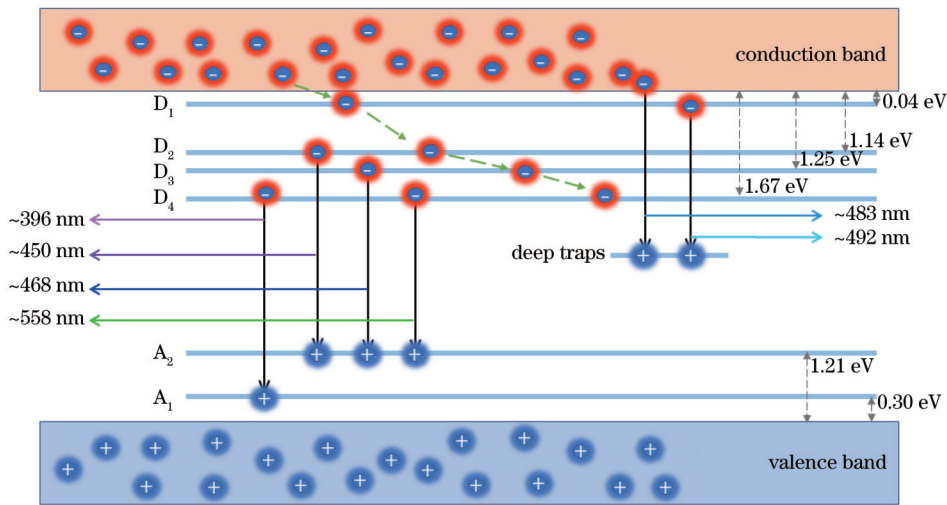


图 5 氮气气氛退火样品的载流子跃迁发光示意图
Fig. 5 Schematic diagram of carrier transition luminescence of sample annealed in nitrogen atmosphere

图 6 为 3 种气氛退火样品的 I - V 特性测试结果。由图 6(a) 中的 I - V 曲线的斜率可知, 氮气、空气和氧气气氛退火的样品电阻依次增大, 样品平均电阻值分别为 $5.32 \times 10^9 \Omega$ 、 $9.19 \times 10^9 \Omega$ 和 $5.83 \times 10^{10} \Omega$, 如图 6

(b) 所示。电阻值与光致发光谱的紫外-蓝光波段发光强度呈相关性。在金属氧化物中, 氧空位缺陷会在带隙中产生深陷阱能级, 以使激活的电子能够移动。因此, 随着氧空位缺陷的增多, Ga_2O_3 薄膜可以产生的自

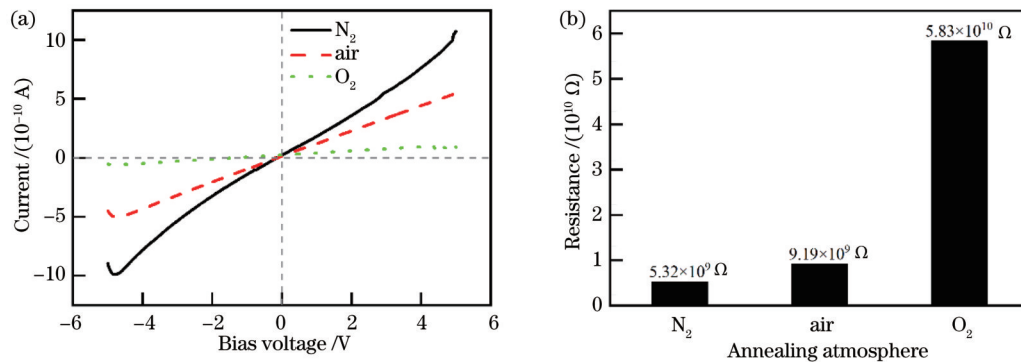
表 1 不同气氛退火的样品缺陷能级分布情况表

Table 1 Distribution of defect energy levels of samples annealed in different atmosphere

Annealing atmosphere	E_g / eV	E_{D1} / eV	E_{D2} / eV	E_{D3} / eV	E_{D4} / eV	E_{A1} / eV	E_{A2} / eV
N ₂	5.10	0.04	1.14	1.25	1.67	0.30	1.21
Air	5.07	0.04	1.11	1.22	1.64	0.30	1.21
O ₂	5.18	0.04	1.22	1.33	1.75	0.30	1.21

由载流子增多,从而减小电阻。氮气气氛退火的样品电阻最小可能是由于薄膜内部参与辐射复合的相关缺陷最多且薄膜致密性较好;空气气氛退火的样品的薄膜内部参与辐射复合的相关缺陷减少且存在较多孔隙,电阻有所增大;氧气气氛退火的样品薄膜致密

性较好,但薄膜内部参与辐射复合的相关缺陷最少,导致薄膜电阻最大。由此可见,当Ga₂O₃薄膜致密性较好时,其电阻主要与薄膜内部参与辐射复合的缺陷相关^[14],选择氮气气氛退火能够提高Ga₂O₃薄膜的导电能力。

图 6 不同气氛退火样品的 I - V 测试结果。(a) I - V 特性曲线图;(b) 平均电阻值变化图Fig. 6 I - V results of annealed samples in different atmosphere. (a) I - V characteristic diagram; (b) variation of average resistance

4 结 论

采用溶液法在石英玻璃衬底上旋涂 Ga₂O₃ 薄膜,并在氮气、空气和氧气三种气氛中进行 1100 °C 高温退火。XRD、SEM、UV-Vis、PL 及 I - V 结果表明:1) 氮气、空气和氧气气氛退火的薄膜,结晶尺寸分别为 23.5 nm、24.9 nm 和 28.1 nm,对日盲紫外光均有较好的选择吸收性,禁带宽度分别为 5.10 eV、5.07 eV 和 5.18 eV,其受主能级及施主能级 D₂、D₃ 和 D₄ 均属于深能级,不利于导电,其电阻分别为 5.32 × 10⁹ Ω、9.19 × 10⁹ Ω 和 5.83 × 10¹⁰ Ω;2) 氮气气氛退火薄膜的致密性与均匀性最优,薄膜最厚,厚度为 222 nm,且其内部参与辐射复合的缺陷最多,因此其电阻最小;3) 在退火温度为 1100 °C、退火时间为 1 h 的退火条件下,氮气气氛退火的 Ga₂O₃ 薄膜是最佳的,其具有较优的形貌组织、光学特性和电学性能,有望应用于电子与光电子等器件。

参 考 文 献

- [1] 王江, 罗林保. 基于氧化镓日盲紫外光电探测器的研究进展[J]. 中国激光, 2021, 48(11): 1100001.
Wang J, Luo L B. Advances in Ga₂O₃-based solar-blind ultraviolet photodetectors[J]. Chinese Journal of Lasers, 2021, 48(11): 1100001.
- [2] Boschi F, Bosi M, Berzina T, et al. Hetero-epitaxy of ϵ -Ga₂O₃ layers by MOCVD and ALD[J]. Journal of Crystal Growth, 2016, 443: 25-30.
- [3] Wang J, Ye L J, Wang X, et al. High transmittance β -Ga₂O₃ thin films deposited by magnetron sputtering and post-annealing for solar-blind ultraviolet photodetector[J]. Journal of Alloys and Compounds, 2019, 803: 9-15.
- [4] Zade V, Makeswaran N, Boyce B L, et al. Structural and mechanical properties of nanocrystalline Ga₂O₃ films made by pulsed laser deposition onto transparent quartz substrates[J]. Nano Express, 2021, 2(2): 020006.
- [5] Hu H Z, Wu C, Zhao N, et al. Epitaxial growth and solar-blind photoelectric characteristic of Ga₂O₃ film on various oriented sapphire substrates by plasma-enhanced chemical vapor deposition[J]. Physica Status Solidi (a), 2021, 218(11): 2100076.
- [6] Park T, Kim K, Hong J. Effects of drying temperature and molar concentration on structural, optical, and electrical properties of β -Ga₂O₃ thin films fabricated by sol-gel method[J]. Coatings, 2021, 11(11): 1391.
- [7] Yu M, Lü C D, Yu J G, et al. High-performance photodetector based on sol-gel epitaxially grown α/β Ga₂O₃ thin films[J]. Materials Today Communications, 2020, 25: 101532.
- [8] Muniz F T L, Miranda M A R, dos Santos C M, et al. The Scherrer equation and the dynamical theory of X-ray diffraction [J]. Acta Crystallographica Section A, 2016, 72(3): 385-390.
- [9] Binet L, Gourier D. Origin of the blue luminescence of β -Ga₂O₃ [J]. Journal of Physics and Chemistry of Solids, 1998, 59(8): 1241-1249.
- [10] Dong L P, Jia R X, Xin B, et al. Effects of oxygen vacancies on the structural and optical properties of β -Ga₂O₃[J]. Scientific Reports, 2017, 7: 40160.
- [11] Harwig T, Kellendonk F. Some observations on the photoluminescence of doped β -galliumsesquioxide[J]. Journal of Solid State Chemistry, 1978, 24(3/4): 255-263.
- [12] Su Y L, Guo D Y, Ye J H, et al. Deep level acceptors of Zn-Mg divalent ions dopants in β -Ga₂O₃ for the difficulty to p -type conductivity[J]. Journal of Alloys and Compounds, 2019, 782:

- 299-303.
- [13] 王丹, 王晓丹, 马海, 等. Ga₂O₃材料的掺杂研究进展[J]. 激光与光电子学进展, 2021, 58(15): 1516025.
Wang D, Wang X D, Ma H, et al. Progress of doping in Ga₂O₃ materials[J]. Laser & Optoelectronics Progress, 2021, 58(15): 1516025.
- [14] Zhu W H, Xiong L X, Si J W, et al. Influence of deposition temperature on amorphous Ga₂O₃ solar-blind ultraviolet photodetector[J]. Semiconductor Science and Technology, 2020, 35(5): 055037.

Effect of Annealing Atmosphere on Structure and Properties of Gallium Oxide Films

Tao Zhiwen¹, Mao Zining², Xu Jiaxiong^{2*}

¹School of Materials and Energy, Guangdong University of Technology, Guangzhou 510006, Guangdong, China;

²School of Integrated Circuits, Guangdong University of Technology, Guangzhou 510006, Guangdong, China

Abstract

Objective Ga₂O₃ exhibits remarkable properties, including broad bandgap, high breakdown field strength, high Baliga quality factor, robust thermal stability, and favorable optical absorption characteristics. These distinctive attributes render it highly suitable for power devices, solar-blind ultraviolet (UV) detection, and UV light-emitting applications. To date, reports concerning Ga₂O₃ thin film synthesis via solution-based methods are comparatively scarce. Pulsed laser deposition and radio frequency sputtering entail costly equipment, while chemical vapor deposition exhibits a relatively low deposition rate. Conversely, solution-based approaches offer benefits encompassing minimal environmental impact and cost, procedural simplicity, and the capacity to yield large and uniformly coated surfaces. However, challenges endure the Ga₂O₃ film synthesized via the solution method, manifesting as reduced crystallinity and inadequate absorption of solar-blind UV light. The content of impurities in precursor solutions, Ga³⁺ concentration, film drying and annealing temperatures, as well as the ambient atmosphere, collectively influence the impurity content, crystallinity, and surface morphology of Ga₂O₃ films, consequently shaping their optical and electrical traits. To mitigate impurities in the solution, we employ 1, 2-diaminopropane containing two amino groups as a stabilizer and devise precursor solutions featuring elevated Ga³⁺ concentrations to curtail the usage of reagents beyond gallium sources. Elevated drying and annealing temperatures are harnessed to amplify film crystallinity. Furthermore, we delve into the crystalline attributes, surface morphology, optical characteristics, bandgap properties, and electrical performance disparities among Ga₂O₃ films subjected to annealing within nitrogen, air, and oxygen environments, simultaneously probing the defect energy levels within these films.

Methods In this investigation, 2-methoxyethanol, gallium nitrate hydrate, and 1, 2-diaminopropane function as a protective solvent, a metal precursor, and a stabilizer respectively to maintain sol stability. This results in a precursor solution with a Ga³⁺ molar concentration of 2.0 mol/L. The precursor solution is applied via spin-coating onto quartz glass substrates, followed by being dried at 200 °C. Subsequently, annealing at 1100 °C for 1 h takes place under nitrogen, air, and oxygen atmospheres, utilizing a tube furnace. X-ray diffraction analysis is performed to assess the crystal structure of the film across different annealing atmospheres. Scanning electron microscopy is employed to characterize film morphology. UV-Vis spectrophotometry is utilized to gather transmittance and reflectance spectra. Photoluminescence spectroscopy is applied to scrutinize the luminescent properties of the films under varying annealing conditions. Small-area ion sputtering is utilized to establish Au electrode contacts on the surface of the Ga₂O₃ film, and the *I-V* characteristics of the Ga₂O₃ film are subjected to testing.

Results and Discussions After being annealed in nitrogen, air, and oxygen atmospheres, the Ga₂O₃ films display pronounced crystallinity, featuring average crystal sizes of 23.5 nm, 24.9 nm, and 28.1 nm, respectively (Fig. 1). Nitrogen-annealed Ga₂O₃ films show the highest density, the most uniform morphology, and the greatest thickness of 222 nm (Fig. 2). The films exhibit transmittance exceeding 80% within the visible light spectrum while allowing less than 10% transmission of 190 nm UV light, indicating favorable selective absorption of solar blind UV light [Fig. 3(b)]. In addition, the bandgap widths of Ga₂O₃ films annealed in nitrogen, air, and oxygen atmospheres are 5.10 eV, 5.07 eV, and 5.18 eV, respectively [Fig. 3(d)]. Photoluminescence spectra disclose that nitrogen-annealed Ga₂O₃ films emit the most intense luminescence, suggesting an abundance of radiative recombination defects. The defects potentially stem from heightened gallium or oxygen vacancies due to reduced crystallinity. In contrast, oxygen-annealed Ga₂O₃ films exhibit

feeble luminescence, signifying diminished radiative recombination defects and effective suppression of UV-blue light emission (Fig. 4). Defect energy levels in Ga_2O_3 films are scrutinized via photoluminescence spectra (Fig. 5). Comparable analyses for other samples unveil a correlation between positions of donor energy levels and bandgap width (Table 1). It can be obtained from the I - V characteristic curve that the resistance of the Ga_2O_3 films annealed in nitrogen, air, and oxygen atmospheres is $5.32 \times 10^9 \Omega$, $9.19 \times 10^9 \Omega$, and $5.83 \times 10^{10} \Omega$, respectively. By comparing the resistances of diverse samples, a link between resistance alterations and photoluminescence intensities is revealed (Fig. 6). When the Ga_2O_3 film demonstrates favorable density, its resistance primarily hinges on internal radiative recombination defects. Consequently, nitrogen-annealed Ga_2O_3 films exhibit augmented conductivity.

Conclusions We employ a solution-based approach to deposit Ga_2O_3 films on quartz glass substrates and conduct high-temperature annealing at 1100°C within nitrogen, air, and oxygen atmospheres. The outcomes from XRD, SEM, UV-Vis, PL, and I - V assessments are as follows. 1) Films annealed in nitrogen, air, and oxygen atmospheres exhibit elevated crystallinity, featuring average crystal sizes of 23.5 nm, 24.9 nm, and 28.1 nm, respectively. They demonstrate preferable absorption of selective solar-blind UV light with bandgap widths of 5.10 eV, 5.07 eV, and 5.18 eV, respectively. Moreover, these films annealed in nitrogen, air, and oxygen atmospheres manifest elevated resistances attributed to the participation of deep energy levels D_2 , D_3 , and D_4 as donors, yielding resistances of $5.32 \times 10^9 \Omega$, $9.19 \times 10^9 \Omega$, and $5.83 \times 10^{10} \Omega$, respectively. 2) Films annealed in nitrogen show superior density, uniformity, and thickness (222 nm), concurrently presenting heightened radiative recombination defects, which in turn result in diminished resistance. 3) Under the annealing condition of 1100°C for 1 h, nitrogen-annealed Ga_2O_3 films evince superior morphology, optical properties, and electrical performance, unveiling their potential for electronic and optoelectronic applications.

Key words thin films; gallium oxide film; annealing atmosphere; solution method; defect level; film properties